ISSN 2579-7069

Time Series Forecasting of Environmental Dynamics in Urban Ecotourism Forest Using Deep Learning

Ade Rahmat Iskandar[1], Arif Imam Suroso[2,*], Irman Hermadi[3], Lilik Budi Prasetyo[4]

[1,3]*School of Data Science, Mathematics and Informatics, IPB University, Bogor, West Java, Indonesia, 16680*

[2]*School of Business, IPB University, Bogor, West Java, Indonesia, 16680*

[4]*Faculty of Forestry, IPB University, West Java, Indonesia, 16680*

[1]*Bachelor of Information Systems, Faculty of Industrial Engineering, Center of Excellence (CoE), Digital Intelligent Enterprises (DIEN), Telkom University, Jakarta, Indonesia, 12970*

(Received: June 22, 2025; Revised: August 20, 2025; Accepted: November 15, 2025; Available online: December 1, 2025)

Abstract

Time Series Forecasting of Environmental Dynamics in urban forests is quite challenging, unless new approaches such as deep learning and remote sensing are employed. Deep learning-based time series algorithms offer robust scientific capabilities for forecasting and assessing sustainability trends using sequential data. Among these, Long Short-Term Memory (LSTM), Gated Recurrent Unit (GRU), and Bidirectional LSTM (BiLSTM) have gained widespread adoption across various predictive modeling domains. In the present research, these algorithms are employed to analyze urban forest raster data derived from the Srengseng Ecotourism Forest, located in West Jakarta, Indonesia. The present study focuses on predicting the temporal patterns of key spatial indicators: Normalized Difference Vegetation Index (NDVI), Land Surface Temperature (LST), and Forest Cover Density (FCD) in the Srengseng urban ecotourism forest area, spanning the years 2014 to 2024, through the application of LSTM, GRU, and BiLSTM deep learning architectures. The methodology used in this study is a combined approach involving remote sensing and deep learning. Spatial data were acquired through the delineation of a high-precision polygon of Srengseng Urban Forest using Google Earth Pro and Google Earth Engine (GEE). GeoTIFF datasets of NDVI, LST, and FCD for the years 2014–2024 were processed using Python-based modeling scripts. Model performance was evaluated through a comparative analysis of LSTM, GRU, and BiLSTM in predicting temporal trends in these ecological indicators. The results of this study show that the Bidirectional LSTM (BiLSTM) consistently demonstrated superior performance to predict all the data spatially, with scores of 0.94 for NDVI, 0.90 for FCD, and 0.85 for LST. Followed by LSTM that predicts NDVI (0.87), FCD (0.89), LST (0.83), as well as GRU, which can estimate spatial data NDVI (0.86), FCD (0.89), and LST (0.85). These results outperformed the predictive accuracy of both the standard LSTM and GRU models.

Keywords: Data Analytics, Deep Learning, Ecotourism, Urban Forest, Remote Sensing, Spatial Data, Time Series

1. Introduction

The Srengseng Urban Ecotourism Forest in West Jakarta, Indonesia, is still managed using conventional approaches. Despite being the focus of various environmental studies, public awareness of its existence and ecological functions remains limited, particularly among Jakarta, Depok, and Bekasi communities. Therefore, historical datasets from Srengseng are crucial for predicting the vegetation index, forest canopy density, and land surface temperature, which serve as key indicators for evaluating ecological comfort in urban ecotourism. Deep learning–based approaches offer a robust framework to transform these spatial datasets into valid scientific evidence that can inform evidence-based decision-making by the Jakarta Department of Parks and Urban Forestry.

Applying time series deep learning algorithms such as LSTM, GRU, and BiLSTM plays a critical role in the sustainable management of urban ecotourism forests. These models enable accurate forecasting of key environmental indicators, including NDVI, Forest Cover Density (FCD), and Land Surface Temperature (LST), thus supporting early detection of vegetation degradation and microclimate changes. The predictive insights derived from these models provide a robust data-driven basis for decision-making in conservation planning, visitor capacity adjustment, and climate-

***Corresponding author: Arif Imam Suroso (arifimamsuroso@apps.ipb.ac.id)**
DOI: https://doi.org/10.47738/jads.v7i1.1029

ISSN 2579-7069

adaptive ecotourism strategies. As a result, integrating deep learning into forest management systems contributes to the advancement of intelligent and resilient urban ecotourism development.

A study that evaluates five Jakarta urban forests, including Srengseng, uses 49 plot inventories and semi-structured interviews and i-Tree Eco to quantify structure, carbon services, and management performance against regulations. Results indicate >50% of trees are in fair condition and an estimated gross carbon sequestration of ~184.8 t C yr^{-1}; Srengseng shows the highest leaf area density but a projected decline in leaf area under mortality scenarios. Management and governance constraints, such as limited planning, uneven staffing, and budget reductions, hamper outcomes despite replanting and community engagement. The authors recommend stronger master planning, stable funding/workforce, and long-term monitoring to optimize urban-forest benefits for Jakarta's low-carbon city agenda [1]. Urban air pollution remains a persistent challenge, and this study quantified the magnitude and economic value of pollutant removal by urban trees and shrubs across the contiguous United States. Using hourly dry deposition flux modeling with 1994 meteorology and pollutant observations from 55 cities, together with resistance-based canopy parameters, the authors estimated the removal of O3, PM10, NO2, SO2, and CO. The analysis indicates total annual removal of approximately 711,000 tons with an externality value near US$3.8 billion, while average city-scale hourly concentration reductions are typically below 1 percent. These results support the integration of strategic urban canopy management into air quality planning as a complementary mitigation measure [2].

The study highlights the lack of accurate data for effective urban forest management in Jakarta, where green spaces remain below national and regional targets. The research aimed to assess tree diversity and vegetation structure as a scientific basis for long-term monitoring. Using 49 field plots across five urban forests, data on tree characteristics were collected and analyzed with the i-Tree Eco program. Results showed moderate diversity (Shannon index 2.1–3.0), dominance of exotic species, and recommended enriching native trees to strengthen sustainable management [3]. A study addresses rapid land use change, deforestation, and biodiversity loss in Indonesian cities, highlighting the urgent need for sustainable green spaces. The objective was to review scientific studies on landscape ecology and urban biodiversity to support conservation and ecological networks. The authors employed literature review and case studies in Jakarta, Bogor, and Sentul City, examining tree species composition, green open space distribution, and ecological connectivity. Results indicate high biodiversity potential in urban parks and home gardens, but dominance of exotic species, stressing the importance of native species, ecological networks, and community-based green city programs for long-term sustainability [4].

A study addresses the lack of updated global analyses on the NDVI–LST relationship for understanding vegetation–climate feedback under climate change. The objective was to assess temporal and spatial correlations between NDVI and LST at a global scale from 2000 to 2024. Using MODIS NDVI (1 km, 16-day) and MODIS LST (1 km, daily) datasets, a pixel-level correlation analysis was conducted. Results show that 20% of global pixels exhibit significant correlations, with 80.4% being negative, which highlights vegetation's cooling effect, while distinct latitudinal peaks indicate stronger correlations in tropical/subtropical southern regions and temperate northern zones [5]. A study that examined the spatiotemporal dynamics of Land Surface Temperature (LST) and Land Cover (LC) in Prešov, Slovakia, by downscaling Landsat-8/9 thermal data with Sentinel-2 indices and applying machine learning classifiers. Their findings indicate that random forest outperformed support vector machines in classification accuracy (up to 93.2%), while significant LST increases were observed in newly developed roads and industrial zones. The study highlights the strong influence of LC transformation on urban heat island intensification in medium-sized cities [6].

The study highlights the challenge of limited high-resolution thermal data in hot, arid urban areas such as Yazd, Iran, where urban heat islands exacerbate climate impacts. The objective was to model and estimate LST using Landsat-8 images and machine learning algorithms across contrasting summer and winter seasons. Six models were tested via AutoML, integrating spectral indices (NDVI, NDBI, albedo, etc.) and spatial features, with DisTrad downscaling applied to thermal bands. Results showed that Gradient Boosting Machine (GBM) achieved the best accuracy (RMSE 0.27–0.32 °C), with albedo and NDVI as the most influential predictors, providing reliable seasonal LST maps to support urban climate resilience strategies [7].

Urban green space dynamics in five major Indonesian cities, namely Jakarta, Bandung, Yogyakarta, Surabaya, and Semarang, have been assessed using Sentinel-2 imagery and vegetation indices (NDVI and EVI) within the Google Earth Engine (GEE) environment. The study aimed to produce accurate vegetation cover maps to inform sustainable urban development. By integrating Sentinel-1 and Sentinel-2 data with vegetation indices, the analysis achieved a classification accuracy of 95.21% and a Kappa coefficient of 0.91. These findings demonstrate the efficacy of remote sensing and cloud-based geospatial platforms for monitoring urban environmental changes [8]. A qualitative

investigation was conducted to evaluate Cultural Ecosystem Services (CESs) of urban forests by analyzing user-generated content in the form of blog narratives. This approach emphasizes the importance of complementing quantitative assessments with qualitative methods to capture place-based values, emotions, and experiences. Drawing on narrative data, the study explored public perceptions and cultural meanings associated with urban forests, with a specific focus on Bukhansan National Park in Korea. The results underscore the value of digital content in assessing CESs and offer insights into enhancing participatory and culturally informed urban forest management [9].

A comparative investigation across nine European countries explored how nature conservation principles are integrated into urban forest management, using in-depth interviews with 42 national experts and forestry practitioners. The study identified strategies for aligning ecological conservation with urban forestry objectives. In a related context, research conducted in Puerto Rico examined environmental attitudes and levels of community participation, with particular attention to residents' Willingness to Pay (WTP) for sustainability programs in urban forest management. These findings collectively highlight the importance of participatory and context-sensitive approaches in advancing urban forest sustainability [10]. Forest change detection in the Southern Mountain Corridor of China has been conducted using cloud-based Landsat imagery on the GEE platform. The study analyzed spatial and temporal forest disturbances and identified their driving forces to support sustainable forest management and national dual carbon objectives. The methodology combined the LandTrendr algorithm for temporal change detection with Random Forest classification to determine disturbance factors. The model achieved a classification accuracy of 82.48% and a Kappa coefficient of 0.70, reflecting strong performance in attributing forest change dynamics [11].

Forest canopy height mapping in metropolitan France was conducted using high-resolution remote sensing data and five machine learning-based predictive models. The objective was to evaluate inter-model prediction variability and quantify spatial uncertainty using the Bayesian Model Averaging (BMA) framework. Findings revealed that model performance was significantly affected by topographic variation, vertical forest stand structure, and land ownership types. Among the tested approaches, the model incorporating dominant spatial structure provided the most consistent and accurate canopy height predictions, outperforming individual models in terms of overall predictive reliability [12]. Recent developments in proximal remote sensing technologies, specifically optical sensors deployed near the surface of ecosystems, have been reviewed to improve the spatial and temporal resolution of monitoring ecosystem structure, function, and fluxes. The primary aim was to bridge the observational scale gap between fine-resolution, ground-based measurements and global satellite-based observations within ecological and climate research. The review systematically examined methods, including LiDAR, Solar-Induced Fluorescence (SIF), spectral reflectance, and thermal infrared sensing, offering recommendations for enhancing data interoperability. While no quantitative metrics were reported, the analysis emphasizes the potential of integrating proximal sensing data into satellite model validation frameworks for improved environmental monitoring [13].

The performance of deep learning models, namely Long Short-Term Memory (LSTM) and Bidirectional LSTM (BiLSTM), was evaluated for predicting non-stationary trends in the Normalized Difference Vegetation Index (NDVI) in Northwest Tunisia using MODIS satellite time series data (2001–2017). The dataset was partitioned into training, testing, and validation subsets, with modeling conducted using standardized parameters in MATLAB. Results revealed that BiLSTM outperformed LSTM in overall predictive accuracy, achieving a minimum RMSE of 0.034 and an R^2 score of 0.96. However, LSTM showed greater sensitivity to vegetation disturbances driven by anthropogenic factors. These findings suggest that model selection should consider the specific temporal and disturbance characteristics of the input data, with BiLSTM demonstrating superior capability in capturing complex and dynamic vegetation patterns [14]. To enhance the precision of soybean yield prediction at the county level in the United States, a novel deep learning model, 3D-ResNet-BiLSTM, was developed. Addressing the limitations of previous models and coarse-resolution input data, the approach leveraged spatiotemporal features extracted from Sentinel-1, Sentinel-2, and Daymet climate datasets, all processed through the Google Earth Engine platform. Model training was conducted on 2019–2020 data and tested against independent 2021 observations. The proposed architecture achieved an R^2 of 0.79 and RMSE of 5.56 bushels/acre, outperforming conventional methods and demonstrating strong predictive accuracy and robustness even under limited training data scenarios. These findings underscore the potential of hybrid deep learning frameworks for timely and reliable crop yield forecasting in support of food security initiatives [15].

A deep learning framework combining Convolutional Neural Networks (CNN) and LSTM was developed to predict spatiotemporal variations of the NDVI across China. Designed to support vegetation monitoring under conditions of climate change and environmental stress, the model integrates spatial feature extraction with CNN and captures temporal dependencies through LSTM. Meteorological variables, including temperature and rainfall from 2000 to 2015, were used to train the model, which was subsequently applied to forecast NDVI values for 2016. The results

demonstrated high predictive accuracy, achieving an R^2 score of 0.91 and RMSE of 0.03, confirming the model's effectiveness in modeling dynamic vegetation responses over time [16]. Rapid urban expansion in the Beijing–Tianjin–Hebei region has posed severe ecological and planning challenges, while traditional cellular automata models struggle to capture complex spatial dependencies and human decision-making. To address this gap, the study proposes an Urban Expansion Scenario Prediction (UESP) model that integrates graph attention networks, vector cellular automata, and agent-based modeling using multi-source big data. The framework dynamically mines transition rules, incorporates resident, traffic, and government behaviors, and simulates four policy-oriented development scenarios. Results show that the model achieves high accuracy (overall accuracy 0.925, Kappa 0.878, FoM 0.048) and demonstrates that ecological and farmland protection policies can effectively mitigate urban sprawl, whereas economic growth–driven expansion may intensify land pressure and ecological degradation [17].

Rapid environmental changes and human activities have significantly altered vegetation cover in the Yangtze River Basin, yet traditional monitoring approaches face limitations in capturing spatiotemporal dynamics. To address this, the study develops a deep learning framework integrating CNN-BiLSTM with an attention mechanism, combined with multiple environmental factors, to predict and analyze vegetation indices (NDVI, EVI, and kNDVI). Using multi-source remote sensing and meteorological data from 2001 to 2020, the model achieved high accuracy with R^2 values exceeding 0.95, demonstrating strong capability in predicting vegetation patterns. The results reveal clear spatiotemporal heterogeneity, showing that precipitation and temperature are dominant drivers, thereby providing valuable insights for regional ecological management and sustainable land-use planning [18].

A time series prediction model based on Bidirectional Long Short-Term Memory networks has been enhanced with a Multi-Scale Local Attention Mechanism (MLAM) to address challenges associated with local information loss and temporal noise in sensor-based datasets. The proposed architecture integrates bidirectional temporal feature extraction with localized attention across short-, mid-, and long-term scales, enabling improved sensitivity to complex and dynamic temporal patterns. Evaluations conducted on public benchmark datasets demonstrate that the BiLSTM-MLAM model outperforms standard models, including GRU, Transformer, and unidirectional LSTM, in terms of Mean Absolute Error (MAE) and Root Mean Square Error (RMSE), while also exhibiting greater robustness in capturing abrupt data fluctuations [19]. A novel framework integrating deep learning, multi-objective optimization, and equitable adaptation strategies has been proposed for climate-resilient time series prediction. The approach, designed to enhance climate change forecasting and optimize resource allocation, incorporates spatiotemporal attenuation modeling, Graph Neural Networks (GNNs), and real-time feedback mechanisms to dynamically account for spatial and social vulnerabilities. Experimental evaluations across multiple datasets demonstrated strong model performance, with results such as $R^2 = 0.9378$, RMSE = 3.89, and MAE = 3.21 in climate-driven traffic prediction tasks. Furthermore, the model maintained high predictive accuracy across diverse benchmark datasets, including PhysioNet ($R^2 = 0.9215$), WADI ($R^2 = 0.9234$), and WorldClim ($R^2 = 0.9289$), underscoring its robustness and generalizability across domains [20].

An AI-driven framework was developed to convert satellite imagery into decision-support information for precision agriculture and agroindustrial applications. The approach aimed to enhance land use planning by simultaneously maximizing economic returns, reducing carbon emissions, and minimizing land degradation. A Convolutional Neural Network was employed for land classification, while a Genetic Algorithm (GA) was used for multi-objective spatial optimization. The framework efficiently produced Pareto-optimal solutions with low computational overhead, demonstrating its effectiveness in supporting sustainable agro-environmental decision-making [21]. Deep learning models based on U-Net and Convolutional Neural Networks have been applied to detect changes in urban forest cover and monitor urban dynamics using very high-resolution satellite imagery. The aim was to improve the accuracy of automated classification methods in capturing complex spatial variations, particularly within green urban areas. The model demonstrated high classification performance, achieving an overall accuracy of 96.5%, with a precision of 94.2%, a recall of 95.6%, and an F1-score of 94.9% in identifying land cover changes. These results highlight the effectiveness of deep learning approaches for fine-scale urban environmental monitoring [22].

2. Materials and methods

2.1. Study Area

Srengseng Urban Forest, established in 1995, covers an area of approximately 10.15 hectares and is geographically located at a longitude of 106°45'57.77" E and a latitude of 6°12'18.77" S in West Jakarta, Indonesia. Srengseng Urban Forest offers several advantages as a potential ecotourism site. First, its strategic location near the center of West Jakarta and more than three decades of establishment have resulted in relatively favorable ecological conditions, including

ISSN 2579-7069

higher average vegetation index, canopy cover density, and soil surface temperature compared to other urban forests in Jakarta. Second, the forest has long served as a research site for academics, including lecturers and students from IPB University, highlighting its scientific relevance. Third, the area is supported by adequate facilities and infrastructure, such as infiltration ponds, jogging and pedestrian tracks, and children's playgrounds, while maintaining affordability with an entrance fee of only 3,000 IDR, making ecotourism activities widely accessible.

Figure 1 illustrates the delineated polygon of Srengseng Urban Ecotourism Forest. The polygon was generated using Google Earth Pro to ensure high mapping precision, with the blue line representing the exact boundaries of the urban forest. This delineation enables accurate extraction of spatial data from Landsat 8 imagery through programmatic processing in Google Earth Engine, thereby producing a precise spatial dataset for the Srengseng Urban Ecotourism Forest.

Figure 1. Srengseng Urban Ecotourism Forest.

2.2. Data Acquisition

This research utilizes Landsat 8 OLI/TIRS satellite imagery to extract spatial information on three key ecological indicators: the Normalized Difference Vegetation Index, Forest Cover Density, and Land Surface Temperature within the ecotourism urban forests of Srengseng. High-precision polygon boundaries for the forest area were delineated using Google Earth Pro and exported in KML/KMZ formats. These were subsequently converted into shapefiles (.shp, .shx, .dbf, prj) using QGIS software to serve as spatial vector data. The resulting shapefiles were employed as input boundaries within custom JavaScript-based applications on the Google Earth Engine (GEE) platform, enabling the retrieval and processing of spatial raster data for further analysis.

2.3. Data preparation and processing

In this research, the Google Earth Engine platform was utilized to develop JavaScript-based scripts for the extraction and analysis of NDVI, FCD, and LST values across the Srengseng urban forests. The spatial datasets span a temporal range from 2014 to 2024.The Normalized Difference Index is calculated using the following equation:

$$NDVI = \left(\frac{NIR-RED}{NIR+RED}\right) \quad (1)$$

The Normalized Difference Vegetation Index is a standardized metric ranging from -1 to 1, commonly used to assess vegetation health. In Landsat 8 imagery, NDVI is calculated using reflectance values from the Near-Infrared (NIR) band (Band 5) and the red band (Band 4). Interpretation of NDVI values is guided by the classification indicators presented in table 1.

Table 1. Urban vegetation classes and NDVI value [23]

No	Vegetation Classes	Description	NDVI Value
1	Non-vegetatiton	Barren areas, built-up areas road network	-1 to 0.199
2	Low vegetation	Shrub and grassland	0.2 to 0.5
3	High Vegetation	Temperature and Tropical Urban Forest	0.501 to 1.0

Land Surface Temperature refers to the actual thermal condition of the Earth's surface, representing the temperature of the ground or vegetation canopy. It is influenced by the balance of solar radiation absorbed and emitted by the surface.

 ISSN 2579-7069

In this study, LST was derived using the Single Channel Algorithm (also known as the Mono-Window Algorithm), which is widely applied for thermal infrared data processing [24].

Step 1: involves the radiometric calibration of the thermal band by converting the Digital Number (DN) values to Top-of-Atmosphere (TOA) spectral radiance. This conversion is carried out using the radiometric calibration formula as defined for Landsat thermal bands.

$$L\lambda = ML * DN + AL \tag{2}$$

Lλ: radiance (expressed in W/m² sr μm) is calculated using the radiometric rescaling factor, where ML represents the multiplicative rescaling factor (gain), AL denotes the additive rescaling factor(bias), both of which are provided in the satellite metadata, and DN refers to the digital number obtained from the satellite imagery.

Step 2: converts radiance to brightness temperature or radiance to temperature using Planck's equation.

$$TB = \frac{K2}{ln\left(\frac{K1}{L\lambda}+1\right)} \tag{3}$$

T denotes brightness temperature in Kelvin (K), where Lλ represents calculated radiance (expressed in W/m²·sr·μm), K1 and K2 are thermal calibration constants obtained from the satellite metadata, used in the conversion of radiance to brightness temperature.

Step 3: Land Surface Temperature correction is calculated using surface Emissivity:

$$LST = \frac{TB}{1+(\lambda .\ TB/P).ln^{E}} \tag{4}$$

LST (Land Surface Temperature) is expressed in Kelvin (K), derived from the brightness temperature (Tb) in Kelvin. The parameter λ denotes the peak wavelength of emitted radiance (typically 10.895 μm for Landsat 8). The constant σhc (or ρ) equals 14388 μm·K. Surface emissivity (ε), which typically ranges from 0.95 to 0.99 for dense vegetation, is applied to correct the thermal radiation for land surface characteristics

Step 5: Conversion of digital number to Top-of-Atmosphere Radiance:

$$L\lambda = ML * DN + AL \tag{5}$$

Step 6: Conversion of brightness to temperature:

$$TB = \frac{K2}{ln\left(\frac{K1}{L\lambda}+1\right)} \tag{6}$$

Final Step: Application of the LST Formula Incorporating Surface Emissivity:

$$\text{Final formula, } LST = \frac{TB}{1+(\lambda .\ TB/P).ln^{E}} \tag{7}$$

Forest Cover Density (FCD) represents the proportion of an area covered by forest canopy and is typically expressed as a percentage. In this study, FCD was analyzed within the context of ecotourism urban forests in Srengseng. The estimation of FCD was derived from the Normalized Difference Vegetation Index, a widely accepted and reliable indicator of vegetation health. NDVI-based approaches to estimate FCD offer a non-destructive and efficient means to quantify canopy density over large spatial extents.

Step 1: Calculate Normalized Difference Vegetation, which serves as an indicator of vegetation density based on the reflectance values of the Near Infra Red (NIR) and red bands.

$$VD = \left(\frac{NDVI-NDVImin}{NDVImax-NDVImin}\right) x\ 100 \tag{8}$$

Vegetation Density (VD) is expressed as a percentage (%) and derived from the normalized NDVI values. Specifically, NDVImin and NDVImax represent the minimum and maximum NDVI values within the image, used to scale the NDVI to vegetation density.

Step 2: Compute the Bare Soil Index (BI), an indicator used to quantify the extent of bare soil within the study area.

$$BI = \frac{(RED+SWIR1)-(NIR+BLUE)}{(RED+SWIR1)+(NIR+SWIR)} \quad (9)$$

The red band is acquired from Band 4 of the Landsat 8 OLI sensor. Short-Wave Infrared 1 (SWIR 1), represented by Band 6 (1.57–1.65 µm), is commonly used in remote sensing to detect surface moisture, differentiate soil types, and analyze vegetation characteristics.

Step 3: The Shadow Index (SI) is calculated to estimate shadowed areas, which are typically associated with dense vegetation or terrain variations:

$$SI = \frac{NIR}{RED} \quad (10)$$

The Shadow Index is a spectral-based metric used to identify shadowed regions in satellite imagery, commonly caused by dense forest canopies or tall vegetation.

Step 4: Estimation of the Thermal Index (TI), which serves as an indicator of surface thermal characteristics derived from thermal infrared data

$$TI = \frac{Tmax-T}{Tmax-Tmin} X\ 100 \quad (11)$$

T represents the land surface temperature derived from radiance calculations. Tmax and Tmin indicate the maximum and minimum observed surface temperatures within the Srengseng urban forest areas, respectively.

Step 5 involves the final calculation of Forest Cover Density, which integrates the vegetation density, Bare Soil Index, Shadow Index, and Thermal Index to produce a comprehensive representation of canopy density within the urban forest.

$$FCD = a * VD + b * BI + c * SI + d * TI \quad (12)$$

Forest Cover Density represents the density of forest canopy expressed in percentage (%). The parameters a, b, c, and d denote the respective weights assigned to the Vegetation Density Index, Bare Soil Index, Shadow Index, and Thermal Index. In this study, the weights were derived from a field survey of the Srengseng urban forest.

Forest Cover Density values are interpreted as follows: values below 40% indicate degraded forest or areas with low canopy cover; values between 40% and 70% represent medium-density forest; and values above 70% correspond to dense forest with high canopy density [25] .

Root Mean Square Error (RMSE) is a widely recognized statistical metric used to evaluate model performance, particularly in fields such as meteorology, water quality assessment, and climate-related studies. It measures the average magnitude of the prediction errors by computing the square root of the mean of the squared differences between predicted and observed values. In the RMSE formula, Yi denotes the actual value, $\hat{y}$i represents the predicted value, and N is the total number of data samples. The term (Yi – $\hat{y}i$)2 captures the squared difference between actual and predicted values, ensuring that all errors are treated as positive regardless of direction. Taking the square root of the mean squared errors restores the unit of the original data, allowing for intuitive interpretation of the model's prediction accuracy.

The R^2 score, or coefficient of determination, is a statistical metric that quantifies how well a regression model explains the variance of the dependent variable relative to the independent variables. In machine learning applications, the R^2 score is commonly used to evaluate the predictive performance of regression models. Where Yi denotes the actual value, $\hat{y}i$ represents the predicted value generated by the model, $\bar{y}$ is the mean of the actual values, and N is the total number of data samples.

Figure 2 illustrates the systematic steps involved in implementing research from start to finish. In the initial part, a precision polygon of the Srengseng ecotourism urban forest was created using GEE and QGIS, then a program code was developed based on Google Earth Engine and the Lndsat 8 Satellite to obtain spatial data of NDVI, LST and FCD from 2014 to 2024, preprocessing was carried out on the spatial data to ensure clean and undamaged data, in the next stage, coding was carried out using a comparison of three deep learning algorithms, namely LSTM, BiLSTM and GRU,

ISSN 2579-7069

in the final stage, further data processing was carried out with the best deep learning algorithm, including the creation of contour plots and heatmaps for each spatial data studied.

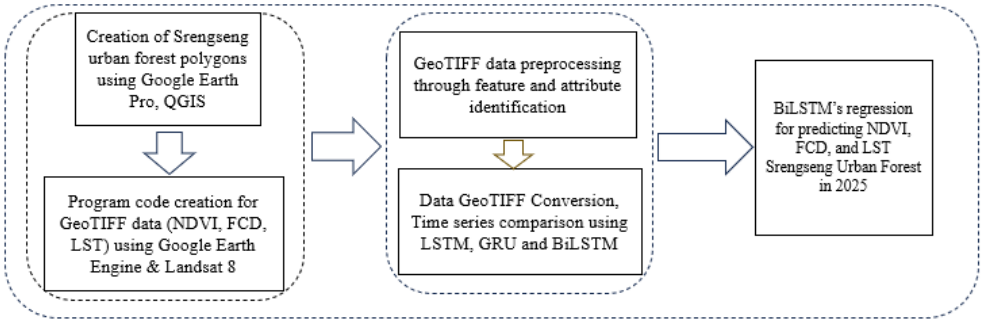

Figure 2. Presents the research workflow describing the overall methodological process.

Figure 3 presents sample outputs generated through the implementation of Google Earth Engine scripts using Landsat 8 satellite imagery to extract NDVI, LST, and FCD spatial data from 2014 to 2024. In addition to visual representations, the resulting GeoTIFF datasets serve as a critical component of this study, providing the primary input for time series deep learning analysis based on the selected algorithm.

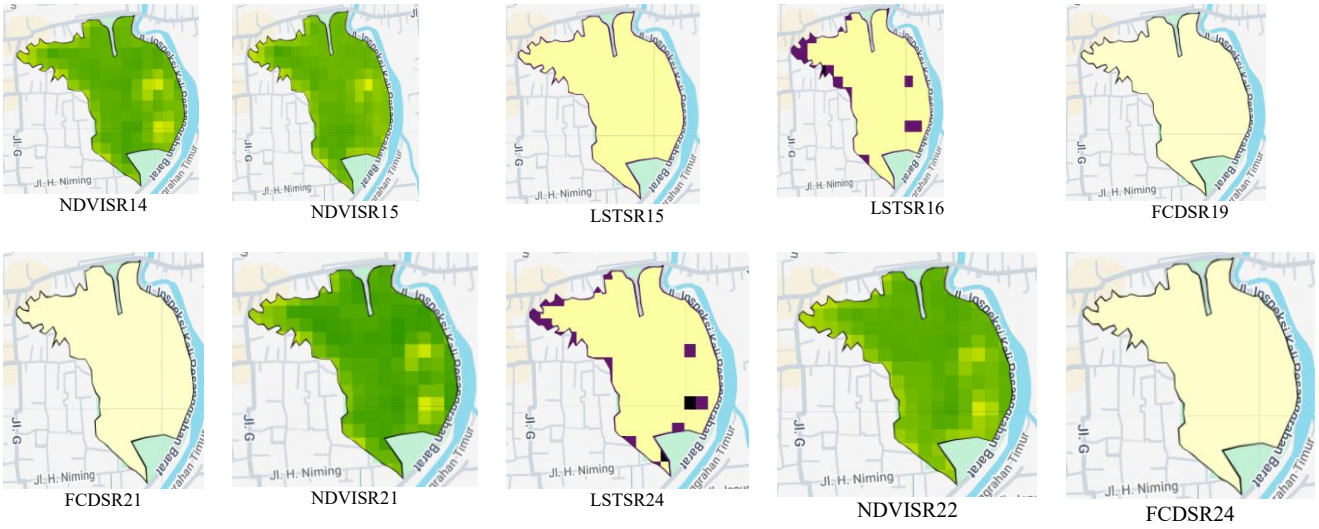

Figure 3. Examples of spatial data for NDVI, LST, and FCD were obtained using Google Earth Engine scripts for the Srengseng Urban Forest, covering the period from 2014 to 2024.

In the subsequent stage, a regression-based comparative analysis was conducted on the spatial time series data of NDVI, FCD, and LST in Srengseng Urban Ecotourism Forest from 2014 to 2024 using three deep learning architectures: Long Short-Term Memory, Gated Recurrent Unit, and Bidirectional LSTM, implemented in Python. Model performance was assessed using standard evaluation metrics, including the coefficient of determination (R^2) and Root Mean Square Error. The primary objective of this analysis was to identify the most accurate model for forecasting NDVI, LST, and FCD values in 2025.

2.4. BiLSTM Time Series Deep Learning

The Bidirectional Long Short-Term Memory algorithm is a deep learning architecture recognized for its strong performance in time series prediction tasks. In contrast to the conventional Long Short-Term Memory model, which processes input data in a unidirectional manner (from past to future), BiLSTM incorporates both forward and backward passes, allowing it to capture temporal dependencies in both directions. This bidirectional learning mechanism often leads to enhanced predictive accuracy, particularly in complex and non-linear time series datasets. The standard LSTM architecture can be mathematically formulated as follows: [14].

 ISSN 2579-7069

$$f_t = \sigma\left(W_f \cdot \left[h_{\{t-1\}}, x_t\right] + b_f\right) \quad (16)$$

The forget gate regulates which information from the previous cell state should be discarded during the update process in the LSTM unit.

$$i_t = \sigma\left(W_i \cdot \left[h_{\{t-1\}}, x_t\right] + b_i\right) \quad (17)$$

The input gate is responsible for controlling how much of the current input and candidate information is allowed to enter and update the internal memory of the LSTM cell.

$$\tilde{C}t = tanh\left(W_C \cdot \left[h_{\{t-1\}}, x_t\right] + b_C\right) \quad (18)$$

The candidate memory content is responsible for generating a set of potential values that can be integrated into the current cell state, subject to regulation by the input gate.

$$C_t = f_t \odot C_{\{t-1\}} + i_t \odot \tilde{C}t \quad (19)$$

The cell state update mechanism is responsible for modifying the previous memory by integrating the retained information with the newly introduced content.

Output Gate

$$o_t = \sigma\left(W_o \cdot \left[h_{\{t-1\}}, x_t\right] + b_o\right) \quad (20)$$

$$h_t = o_t \odot tanh(C_t) \quad (21)$$

The hidden gate represents the hidden state output of the LSTM at time step t, which serves both as a feature for prediction and as input for the subsequent time step.

The BiLSTM architecture can be mathematically expressed using the following formulation[19].

$$\overrightarrow{h}_t = LSTM_f wd(x_t)\ \overleftarrow{h}_t = LSTM_b wd(x_t)\quad h_t = [\overrightarrow{h}_t; \overleftarrow{h}_t]^T \quad (22)$$

$\overrightarrow{h}_t$ This represents the forward LSTM output that captures the input features from the past to the future x_t from time direction t = 1 → T (onward)

$h \leftarrow_t$ This is the output of a backward LSTM that processes the input x_t from the final time step to the initial one t = T → 1 (receding)

$h_t = [\overrightarrow{h}_t; \overleftarrow{h}_t]^T$: The final hidden state h_t is obtained by concatenating the outputs from both the forward and backward LSTM passes, effectively combining temporal features from past and future contexts.

3. Results and Discussion

The performance of the models is evaluated using the coefficient of determination (R^2 score) to assess the predictive accuracy of three deep learning algorithms, namely LSTM, GRU, and BiLSTM, in forecasting urban forest indicators, namely NDVI, LST, and FCD, over the period from 2014 to 2024. The R^2 scores for each algorithm are presented in table 2 and figure 4, while table 3 summarizes the corresponding Root Mean Square Error (RMSE) values.

Table 2. R^2 scores of time series Deep learning comparisons

R^2score indicator	LSTM	GRU	BiLSTM
NDVI1424	0.87	0.86	0.94
LST1424	0.83	0.85	0.85
FCD1424	0.89	0.89	0.90

Table 3. RMSE scores of time series Deep learning comparisons

RMSE indicator	LSTM	GRU	BiLSTM
NDVI1424	0.0236	0.0247	0.0169
LST1424	0.0703	0.0679	0.0674
FCD1424	0.0825	0.0676	0.0795

As shown in figure 4, the BiLSTM time series deep learning model consistently achieves the highest prediction accuracy across all urban forest indicators. Specifically, BiLSTM yields R^2 scores of 0.94 for NDVI (2014–2024), 0.90 for FCD (2014–2024), and 0.85 for LST (2014–2024). In comparison, the LSTM model achieves R^2 values of 0.86,

 ISSN 2579-7069

0.89, and 0.83 for the respective indicators, while the GRU model records R^2 scores of 0.86, 0.89, and 0.85. These results indicate the superior performance of BiLSTM in modeling spatiotemporal patterns of urban forest indicators.

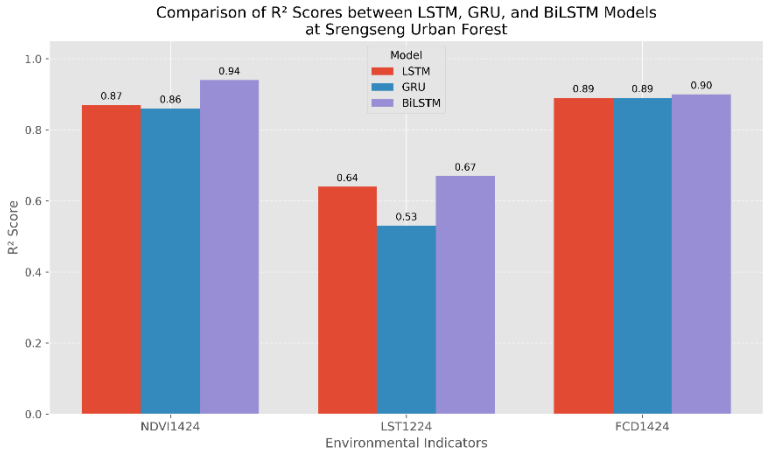

Figure 4. Comparison of prediction accuracy for NDVI, LST, and FCD using LSTM, GRU, and BiLSTM algorithms in Srengseng Urban Forest (2014–2024).

In addition to the R^2 score, the predictive performance of each deep learning algorithm, namely Long Short-Term Memory, Gated Recurrent Unit, and Bidirectional Long Short-Term Memory, was evaluated using the Root Mean Squared Error (RMSE), a widely used metric that quantifies the average magnitude of prediction errors. Table 3 summarizes the RMSE results for three key urban forest environmental indicators: NDVI, LST, and FCD, over the 2014–2024 period. Among the three models, the BiLSTM consistently achieved the lowest RMSE values, with 0.0169 for NDVI, 0.0674 for LST, and 0.0795 for FCD, demonstrating its superior capability in capturing temporal patterns by leveraging bidirectional processing. The LSTM model followed, with RMSE values of 0.0236 (NDVI), 0.0703 (LST), and 0.0825 (FCD), while the GRU model yielded RMSEs of 0.0247, 0.0679, and 0.0676, respectively. These results indicate that BiLSTM provides the most accurate predictions among the tested models for urban forest dynamics. Deep Learning-Based Time Series Results Analysis of Srengseng Urban Forest:

Consistent with the R^2 score and RMSE results reported in Tables 2 and 3, Figure 4 presents the contour plots produced by the three deep learning time series models: BiLSTM, LSTM, and GRU. Among these, the BiLSTM model exhibits the highest predictive accuracy, attributed to its bidirectional architecture that processes input sequences in both forward and backward directions. This structure enables the model to capture not only historical dependencies but also contextual information from future sequences, thereby improving its capacity to learn complex, non-linear, and dynamic patterns in environmental sensor data. These findings highlight the effectiveness of bidirectional integration in enhancing the representation of both short- and long-term temporal dependencies.

Figure 5 illustrates that all three deep learning time series models, namely BiLSTM, LSTM, and GRU, exhibit robust and reliable predictive performance. For NDVI, FCD, and LST spatial datasets, the average accuracy exceeds 89% for NDVI, 89.3% for FCD, and 84.3% for LST, all the data spatial obtained from 2014 to 2024.

The dataset utilized in this study was independently developed through the processing of Landsat 8 satellite imagery on the Google Earth Engine platform. The researchers delineated the Srengseng Urban Forest Ecotourism polygon and extracted multitemporal spatial data to derive three key environmental indicators: NDVI (2014–2024), LST (2014–2024), and FCD (2014–2024). These data products were generated using custom algorithms and spatial computation workflows implemented in Python. As such, the datasets are not publicly available in standard repositories but represent original outputs tailored specifically to this research through machine learning-based spatial analysis.

ISSN 2579-7069

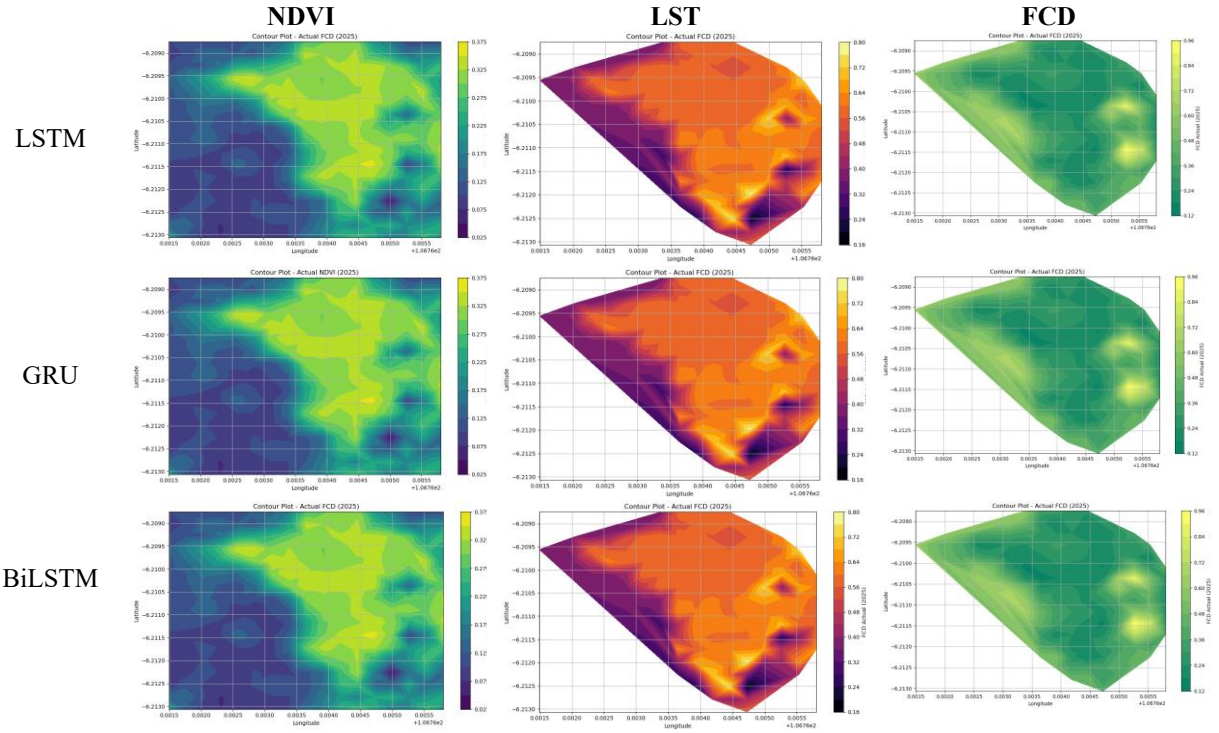

Figure 5. Comparison of prediction accuracy for NDVI, LST, and FCD using LSTM, GRU, and BiLSTM algorithms in Srengseng Urban Forest (2014–2024).

The following is a Python-based program code snippet using a manual tuning concept for BiLSTM, LSTM, and GRU, and successfully increased the accuracy of Land Surface Temperature predictions in the Srengseng urban forest.

Algorithm 1. Snippet using a manual tuning concept for BiLSTM, LSTM, and GRU

```
model = Sequential([
    Bidirectional(LSTM(64, return_sequences=True, dropout=0.2, recurrent_dropout=0.1),
                  input_shape=(L, 1)),
    Bidirectional(LSTM(32, dropout=0.2, recurrent_dropout=0.1)),
    Dense(32, activation='relu'),
    Dropout(0.1),
    Dense(1)
])

model = Sequential([
    LSTM(64, return_sequences=True, dropout=0.2, recurrent_dropout=0.1, input_shape=(L,1)),
    LSTM(32, dropout=0.2, recurrent_dropout=0.1),
    Dense(32, activation='relu'),
    Dropout(0.1),
    Dense(1)
])

model = Sequential([
    GRU(64, return_sequences=True, dropout=0.2, recurrent_dropout=0.1, input_shape=(L,1)),
    GRU(32, dropout=0.2, recurrent_dropout=0.1),
    Dense(32, activation='relu'),
    Dropout(0.1),
    Dense(1)
])
```

The BiLSTM, LSTM, and GRU models were manually tuned by adjusting the number of hidden units, dropout rates, and activation functions, as shown in the modified architecture. Although the tuning process was heuristic rather than systematic, this configuration significantly improved predictive performance on the LST dataset. The results demonstrated higher R^2 values and lower RMSE compared to the baseline models, indicating that even manual hyperparameter adjustments can substantially enhance the accuracy and robustness of spatio-temporal LST prediction.

ISSN 2579-7069

4. Discussion

In this study, the Bidirectional Long Short-Term Memory algorithm achieved the highest predictive performance for estimating the Normalized Difference Vegetation Index, Forest Cover Density, and Land Surface Temperature in the Srengseng ecotourism urban forest. Comparable studies have reported similarly strong results, with NDVI predictions reaching an accuracy of up to 93% using BiLSTM models applied to MODIS satellite data processed in MATLAB [14] Similarly, a study focusing on NDVI prediction using the BiLSTM deep learning algorithm in northern China reported an accuracy of 83%, demonstrating the model's effectiveness in different geographic contexts [16]. Comparative studies evaluating the performance of BiLSTM against various machine learning and deep learning algorithms, including Linear Regression (LR), Random Forest (RF), 1D/2D/3D-ResNet architectures, and hybrid 2D-CNN-LSTM models, have shown that BiLSTM consistently outperforms these approaches in predictive accuracy and temporal feature learning [15].

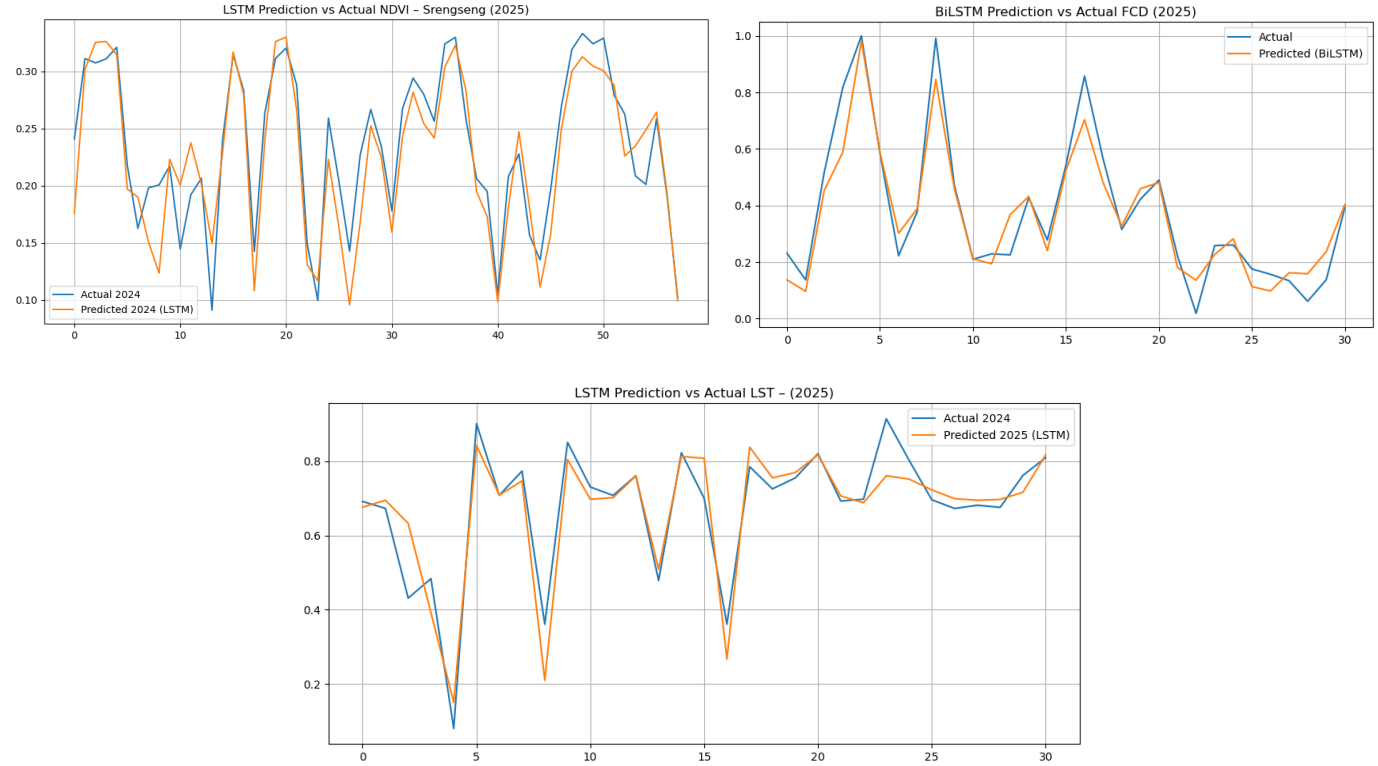

Figure 6. Predicted NDVI, FCD, and LST values for the year 2025 using the Bidirectional Long Short-Term Memory (BiLSTM) deep learning algorithm.

The BiLSTM deep learning algorithm was employed to predict NDVI, FCD, and LST values for the year 2025 using historical data from 2014 to 2024, demonstrating a high level of predictive performance for both indicators. Vegetation and tree health metrics, such as NDVI, are particularly well-suited for analysis due to the availability of relevant Landsat 8 spectral bands (Red and Near-Infrared), which enable accurate object detection. The FCD predictions also yielded strong results, supported by the comprehensive accumulation of a decade's worth of spatial data leading up to the forecast year. Likewise, with LST, BiLSTM deep learning is able to estimate 85% in the Srengseng urban forest.

Compared to FCD and NDVI, predicting LST is more difficult because it is affected by multiple heterogeneous factors such as soil moisture, surface emissivity, atmospheric variability, and urban heat dynamics. These additional influences introduce higher non-linear complexity and temporal fluctuations into the data. In contrast, FCD and NDVI are directly derived from spectral reflectance, making their patterns more stable and easier to model. As a result, LST prediction generally requires more sophisticated models to achieve reliable accuracy. Carrying out the tuning process either manually or using algorithms such as GridSearch can help produce good estimated values on this LST spatial data, as shown in the Python program code snippet for the manual tuning process in Section 3 Results and Discussion.

The Land Surface Temperature dynamics analysis in Srengseng Urban Forest from 2014 to 2024 demonstrates that deep learning models can effectively capture the temporal–spatial variability of urban forest microclimates. In particular, the Bi-directional Long Short-Term Memory model achieved a predictive accuracy of approximately 85%, outperforming traditional approaches in handling sequential dependencies across the ten-year dataset. This result highlights the robustness of BiLSTM in modeling long-term urban forest temperature fluctuations. It provides strong evidence of its potential application in supporting sustainable urban-forest management and ecotourism planning.

Although the deep learning models (BiLSTM, LSTM, and GRU) achieved strong predictive performance for NDVI, FCD, and LST in Srengseng Urban Forest (85–94%), several challenges remain. Spatial heterogeneity, noise from remote sensing data, limited temporal resolution, and irregular human activities around the forest can introduce variability that reduces prediction stability. These factors explain why the accuracy, while generally high, cannot reach perfect levels across all indicators and years.

The results indicate that the bi-directional long short-term memory model achieved slightly better performance than the conventional LSTM and GRU models. This improvement can be attributed to the bidirectional structure of BiLSTM, which processes sequential information from both past and future directions, thereby capturing a more comprehensive temporal dependency within the dataset. While LSTM and GRU are effective in handling long-term dependencies, their unidirectional nature may limit the ability to fully exploit contextual information. Consequently, BiLSTM provides a marginal yet consistent advantage, particularly in modeling complex temporal–spatial dynamics such as urban forest Land Surface Temperature.

5. Conclusion

The comparative results of the three deep learning time series models, namely Long Short-Term Memory, Gated Recurrent Unit, and Bidirectional LSTM, demonstrated similarly high predictive performance. These findings suggest that all three models are capable of generating accurate forecasts when supported by a sufficiently long and representative dataset, ideally spanning at least a decade. In this study, historical data from 2014 to 2024 were utilized to predict the Normalized Difference Vegetation Index, Forest Cover Density, and Land Surface Temperature for the year 2025.

This research confirms the effectiveness of deep learning-based time series models for predicting spatial ecological indicators in urban forest environments. Among the evaluated models, Bidirectional LSTM demonstrated the highest predictive accuracy for NDVI, FCD, and LST. The integration of remote sensing data with a BiLSTM architecture proved to be a reliable approach for modeling temporal dynamics in urban ecological systems. These findings highlight the potential of BiLSTM as a robust tool to support data-driven urban forest management and sustainability planning.

This study provides a significant contribution to forecasting spatial indicators of NDVI, FCD, and LST for 2025 using historical data from 2014 to 2024. The deep learning analysis suggests that the vegetation index may exceed 94%, forest canopy density could approach 90%, and land surface temperature predictions achieve an accuracy of around 85%. These findings offer strong scientific evidence to guide the DKI Jakarta Parks and Urban Forestry Service in maintaining ecological sustainability and improving urban community comfort within the ecotourism context of Srengseng Urban Forest.

6. Declarations

6.1. Author Contributions

Conceptualization: A.R.I., A.I.S., I.H., and L.B.P.; Methodology: A.I.S.; Software: A.R.I.; Validation: A.R.I., A.I.S., I.H., and L.B.P.; Formal Analysis: A.R.I., A.I.S., I.H., and L.B.P.; Investigation: A.R.I.; Resources: A.I.S.; Data Curation: A.I.S.; Writing—Original Draft Preparation: A.R.I., A.I.S., I.H., and L.B.P.; Writing—Review and Editing: A.I.S., A.R.I., I.H., and L.B.P.; Visualization: A.R.I.; All authors have read and agreed to the published version of the manuscript.

6.2. Data Availability Statement

The data presented in this study are available on request from the corresponding author.

6.3. Funding

The authors received no financial support for the research, authorship, and/or publication of this article.

6.4. Institutional Review Board Statement

Not applicable.

6.5. Informed Consent Statement

Not applicable.

6.6. Declaration of Competing Interest

The authors declare that they have no known competing financial interests or personal relationships that could have appeared to influence the work reported in this paper.

References

[1] R. Aulia et al., "Assessing the benefits and management of urban forest in supporting low carbon city in Jakarta, Indonesia," *Biodiversitas*, vol. 24, no. 11, pp. 6151–6159, 2023, doi: 10.13057/biodiv/d241136.

[2] D. J. Nowak, D. E. Crane, and J. C. Stevens, "Air pollution removal by urban trees and shrubs in the United States," *Urban For. Urban Green*., vol. 4, no. 3–4, pp. 115–123, 2006, doi: 10.1016/j.ufug.2006.01.007.

[3] A. Mosyaftiani et al., "Monitoring and analyzing tree diversity using i-Tree eco to strengthen urban forest management," *Biodiversitas*, vol. 23, no. 8, pp. 4033–4039, 2022, doi: 10.13057/biodiv/d230822.

[4] H. S. Arifin and N. Nakagoshi, "Landscape ecology and urban biodiversity in tropical Indonesian cities," *Landsc. Ecol. Eng*., vol. 7, no. 1, pp. 33–43, 2011, doi: 10.1007/s11355-010-0145-9.

[5] E. Rahimi, P. Dong, and C. Jung, "Global NDVI-LST Correlation: Temporal and Spatial Patterns from 2000 to 2024," *Environ*. - MDPI, vol. 12, no. 2, pp. 1–14, 2025, doi: 10.3390/environments12020067.

[6] A. Uhrin and K. Onačillová, "Spatiotemporal analysis of land surface temperature and land cover changes in Prešov city using downscaling approach and machine learning algorithms," *Environ. Monit. Assess*., vol. 197, no. 2, pp. 1-25, .2025, doi: 10.1007/s10661-024-13598-8.

[7] M. Mansourmoghaddam, I. Rousta, H. Ghafarian Malamiri, M. Sadeghnejad, J. Krzyszczak, and C. S. S. Ferreira, "Modeling and Estimating the Land Surface Temperature (LST) Using Remote Sensing and Machine Learning (Case Study: Yazd, Iran)," *Remote Sens*., vol. 16, no. 3, pp. 1-24, 2024, doi: 10.3390/rs16030454.

[8] A. Agustiyara, D. Mutiarin, A. Nurmandi, A. N. Kasiwi, and M. F. Ikhwali, "Mapping Urban Green Spaces in Indonesian Cities Using Remote Sensing Analysis," *Urban Sci*., vol. 9, no. 2, pp. 1–23, 2025, doi: 10.3390/urbansci9020023.

[9] J. Kim and Y. Son, "Assessing and mapping cultural ecosystem services of an urban forest based on narratives from blog posts," *Ecol. Indic*., vol. 129, pp. 1-11, 2021, doi: 10.1016/j.ecolind.2021.107983.

[10] H. Tavárez and L. Elbakidze, "Urban forests valuation and environmental disposition: The case of Puerto Rico," *For. Policy Econ*., vol. 131, pp. 1-6, 2021, doi: 10.1016/j.forpol.2021.102572.

[11] R. Wu, J. Wang, D. Zhang, and S. Wang, "Identifying different types of urban land use dynamics using Point-of-interest (POI) and Random Forest algorithm: The case of Huizhou, China," *Cities*, vol. 114, pp. 1-18, 2021, doi: 10.1016/j.cities.2021.103202.

[12] N. Besic et al., "Remote-sensing-based forest canopy height mapping: some models are useful, but might they provide us with even more insights when combined?," *Geosci. Model Dev*., vol. 18, no. 2, pp. 337–359, 2025, doi: 10.5194/gmd-18-337-2025.

[13] Z. A. Pierrat et al., "Proximal remote sensing: an essential tool for bridging the gap between high-resolution ecosystem monitoring and global ecology," *New Phytol*., vol. 246, no. 2, pp. 419–436, 2025, doi: 10.1111/nph.20405.

[14] M. Rhif, A. Ben Abbes, B. Martinez, and I. R. Farah, "Deep Learning Models Performance for NDVI Time Series Prediction: A Case Study on North West Tunisia," *2020 Mediterr. Middle-East Geosci. Remote Sens. Symp. M2GARSS 2020 - Proc*., no. March, pp. 9–12, 2020, doi: 10.1109/M2GARSS47143.2020.9105149.

[15] M. Fathi, R. Shah-Hosseini, and A. Moghimi, "3D-ResNet-BiLSTM Model: A Deep Learning Model for County-Level Soybean Yield Prediction with Time-Series Sentinel-1, Sentinel-2 Imagery, and Daymet Data," *Remote Sens*., vol. 15, no. 23, pp. 1–20, 2023, doi: 10.3390/rs15235551.

[16] Y. Sun, D. Lao, Y. Ruan, C. Huang, and Q. Xin, "A Deep Learning-Based Approach to Predict Large-Scale Dynamics of Normalized Difference Vegetation Index for the Monitoring of Vegetation Activities and Stresses Using Meteorological Data," *Sustain*., vol. 15, no. 8, pp. 1-21, 2023, doi: 10.3390/su15086632.

[17] Y. Gao, D. Liu, X. Zheng, X. Wang, and G. Ai, "Urban Expansion Scenario Prediction Model: Combining Multi-Source Big Data, a Graph Attention Network, a Vector Cellular Automata, and an Agent-Based Model," *Remote Sens*., vol. 17, no. 13, pp. 1–22, 2025, doi: 10.3390/rs17132272.

[18] Y. Wang et al., "Prediction and Spatiotemporal Dynamics of Vegetation Index Based on Deep Learning and Environmental Factors in the Yangtze River Basin," *Forests*, vol. 16, no. 3, pp. 1-20, 2025, doi: 10.3390/f16030460.

[19] Y. Fan, Q. Tang, Y. Guo, and Y. Wei, "BiLSTM-MLAM: A Multi-Scale Time Series Prediction Model for Sensor Data Based on Bi-LSTM and Local Attention Mechanisms," *Sensors*, vol. 24, no. 12, pp. 1-16, 2024, doi: 10.3390/s24123962.

[20] C. Chen and J. Dong, "Deep learning approaches for time series prediction in climate resilience applications," *Front. Environ. Sci*., vol. 13, no. April, pp. 1–18, 2025, doi: 10.3389/fenvs.2025.1574981.

[21] I. Firdaus, Y. Arkeman, A. Buono and Hermadi, "Satellite image processing for precision agriculture and agroindustry using convolutional neural network and genetic algorithm," *J. Phys. Conf. Ser*., vol. 755, no. 1, pp. 1-7, 2016, doi: 10.1088/1742-6596/755/1/011001.

[22] A. Javed, T. Kim, C. Lee, J. Oh, and Y. Han, "Deep Learning-Based Detection of Urban Forest Cover Change along with Overall Urban Changes Using Very-High-Resolution Satellite Images," *Remote Sens*., vol. 15, no. 17, pp. 1-18, 2023, doi: 10.3390/rs15174285.

[23] H. Hashim, Z. Abd Latif, and N. A. Adnan, "URBAN VEGETATION CLASSIFICATION with NDVI THRESHOLD VALUE METHOD with VERY HIGH RESOLUTION (VHR) PLEIADES IMAGERY," *Int. Arch. Photogramm. Remote Sens. Spat. Inf. Sci. - ISPRS Arch*., vol. 42, no. 4/W16, pp. 237–240, 2019, doi: 10.5194/isprs-archives-XLII-4-W16-237-2019.

[24] M. Wang, Z. Zhang, T. Hu, and X. Liu, "A Practical Single-Channel Algorithm for Land Surface Temperature Retrieval: Application to Landsat Series Data," *J. Geophys. Res. Atmos*., vol. 124, no. 1, pp. 299–316, 2019, doi: 10.1029/2018JD029330.

[25] D. T. Loi, T.-Y. Chou, and Y.-M. Fang, "Integration of GIS and Remote Sensing for Evaluating Forest Canopy Density Index in Thai Nguyen Province, Vietnam," *Int. J. Environ. Sci. Dev*., vol. 8, no. 8, pp. 539–542, 2017, doi: 10.18178/ijesd.2017.8.8.1012.